JOURNAL OF GUIDANCE, CONTROL, AND DYNAMICS
Vol. 15, No. 4, July-August 1992

Nonlinear Inversion Flight Control for a Supermaneuverable Aircraft

S. Antony Snell,* Dale F. Enns,† and William L. Garrard Jr.‡
University of Minnesota, Minneapolis, Minnesota 55455

Nonlinear dynamic inversion affords the control system designer a straightforward means of deriving control laws for nonlinear systems. The control inputs are used to cancel unwanted terms in the equations of motion using negative feedback of these terms. In this paper, we discuss the use of nonlinear dynamic inversion in the design of a flight control system for a supermaneuverable aircraft. First, the dynamics to be controlled are separated into fast and slow variables. The fast variables are the three angular rates and the slow variables are the angle of attack, sideslip angle, and bank angle. A dynamic inversion control law is designed for the fast variables using the aerodynamic control surfaces and thrust vectoring control as inputs. Next, dynamic inversion is applied to the control of the slow states using commands for the fast states as inputs. The dynamic inversion system was compared with a more conventional, gain-scheduled system and was shown to yield better performance in terms of lateral acceleration, sideslip, and control deflections.

Nomenclature

C_i	= aerodynamic force or moment coefficient
C_{i_j}	= aerodynamic force or moment i, derivative due to state or input j
$\bar{c},b$	= mean aerodynamic chord, wing span
I_{ij}	= moment/product of inertia about body axes x, y, and z
L,D,Y	= aerodynamic lift, drag, and side force
l,m,n	= aerodynamic rolling, pitching, and yawing moment
M	= aircraft mass
m_T,n_T	= pitching and yawing moment produced by thrust vectoring control
p,q,r	= body-axis roll, pitch, and yaw rate
$\bar{q}$	= dynamic pressure
S	= reference wing area
T	= engine thrust
T_x,T_y,T_z	= body-axis components of thrust
u,v,w	= body-axis velocity components
V	= aircraft speed
α	= angle of attack, $= \tan^{-1}(w/u)$
β	= sideslip angle, $= \sin^{-1}(v/V)$
γ	= flight-path angle
$\delta_a,\delta_e,\delta_r$	= aileron, canard, and rudder deflection angles
$\delta_T = T_c$	= throttle setting = thrust command
δ_y,δ_z	= lateral and normal thrust vectoring control deflection angles
μ	= bank angle about the velocity vector

Introduction

REFERENCE 1 suggests that considerable tactical advantages can be gained by use of post-stall maneuvering in air-to-air combat situations. A problem is posed in that the aircraft dynamics exhibit significant coupling and nonlinearity when the aircraft operates at high angle of attack and with large angular rates. Reference 2 proposes the use of a gain-scheduled (GS) linear control law. However, it will be demonstrated in this paper that this particular control law has serious shortcomings that would need to be addressed before it could be considered as a practical system for supermaneuvering flight. Instead, an alternative control law was devised that makes use of the dynamic inversion technique.[3,4]

In its most basic, first-order form, dynamic inversion requires that the system have at least as many inputs as states. This is not generally the case in aircraft control systems. This problem was solved by formulating the problem as a two time scale problem. A general approach to order reduction by the two time scale technique is discussed in Refs. 5 and 6. Other researchers have specifically applied two time scale ideas to aircraft systems.[7,8] References 9 and 10 discuss other applications of nonlinear inversion to aircraft flight control. Reference 11 presents nonlinear inversion and decoupling applied to general systems.

In the approach of this paper, the fast dynamics correspond to the states p, q, and r, which are controlled by the five inputs: aileron, canard, rudder, and lateral and normal thrust vectoring control (TVC). Having designed a fast-state controller, a separate, approximate inversion procedure is carried out to design the slow-state controller for α, β, and μ using the commands for p, q, and r as inputs. This model reduction method can only be justified if there is a significant difference in the time scales between the fast and slow states in the open-loop plant. It will be shown later that this is the case with this aircraft model. It is also true for most aircraft.

Figure 1 shows the configuration of the dynamic inversion control laws. The motivation for such an arrangement is that it is assumed that the pilot generates commands for α, μ, and thrust and also commands β to zero. These variables directly control the magnitude and direction of the lift, drag, and thrust vectors. The outer-loop control law is required to give good response in these variables.

The remainder of this paper will discuss the mathematical model, then the fast- and slow-state inversion controllers. This is followed by a comparison of the inversion control law with the gain-scheduled control law of Ref. 2 during a simulated supermaneuver. The paper concludes with plans for future work.

Mathematical Model

The full, six-degree-of-freedom (DOF), nonlinear, rigid-body dynamics are modeled by the following, nine-state sys-

Presented as Paper 90-3406 at the AIAA Guidance, Navigation, and Control Conference, Portland, OR, Aug. 20-22, 1990; received Nov. 2, 1990; revision received Aug. 2, 1991; accepted for publication Aug. 9, 1991.

*Research Assistant, Aerospace Engineering. Student Member AIAA.

†Adjunct Associate Professor, Aerospace Engineering and Mechanics; also Senior Research Fellow, Honeywell Systems and Research Center. Member AIAA.

‡Professor, Aerospace Engineering and Mechanics. Associate Fellow AIAA.

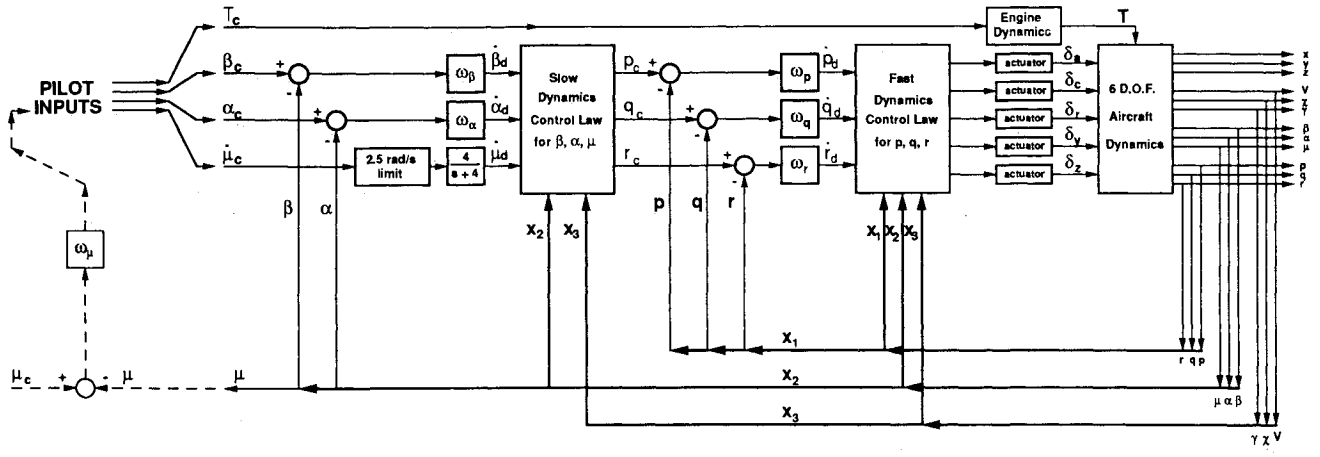

Fig. 1 Configuration of nonlinear dynamic inversion control laws.

tem of equations. No spatial dependence is included in our model, so the three states corresponding to the position in space of the aircraft are decoupled from the nine-state system below:

$$\dot{V} = \frac{1}{M}[-D + (Y + T_y)\sin(\beta) - Mg\sin(\gamma) + T_x\cos(\beta)\cos(\alpha) + T_z\cos(\beta)\sin(\alpha)] \tag{1}$$

$$\dot{\chi} = \frac{1}{MV\cos(\gamma)}\{L\sin(\mu) + (Y + T_y)\cos(\mu)\cos(\beta) + T_x[\sin(\mu)\sin(\alpha) - \cos(\mu)\sin(\beta)\cos(\alpha)]\} - \frac{T_z}{MV\cos(\gamma)}[\cos(\mu)\sin(\beta)\sin(\alpha) + \sin(\mu)\cos(\alpha)] \tag{2}$$

$$\dot{\gamma} = \frac{1}{MV}[L\cos(\mu) - Mg\cos(\gamma) - (Y + T_y)\sin(\mu)\cos(\beta)] + \frac{T_x}{MV}[\sin(\mu)\sin(\beta)\cos(\alpha) + \cos(\mu)\sin(\alpha)] + \frac{T_z}{MV}[\sin(\mu)\sin(\beta)\sin(\alpha) - \cos(\mu)\cos(\alpha)] \tag{3}$$

$$\dot{\beta} = \sin(\alpha)p - \cos(\alpha)r + \frac{1}{MV}[Mg\cos(\gamma)\sin(\mu)] + \frac{1}{MV}[(Y + T_y)\cos(\beta) - \frac{1}{MV}T_x\sin(\beta)\cos(\alpha)] + \frac{1}{MV}[T_z\sin(\beta)\sin(\alpha)] \tag{4}$$

$$\dot{\alpha} = q - \tan(\beta)[\cos(\alpha)p + \sin(\alpha)r] + \frac{1}{MV\cos(\beta)} \times [-L + Mg\cos(\gamma)\cos(\mu)] + \frac{1}{MV\cos(\beta)} \times [-T_x\sin(\alpha) + T_z\cos(\alpha)] \tag{5}$$

$$\dot{\mu} = \sec(\beta)[\cos(\alpha)p + \sin(\alpha)r] - \frac{g}{V}\cos(\gamma)\cos(\mu)\tan(\beta) + \frac{L}{MV}[\tan(\gamma)\sin(\mu) + \tan(\beta)] + \frac{(Y + T_y)}{MV}\tan(\gamma)\cos(\mu)\cos(\beta) + \frac{T_x\sin(\alpha) - T_z\cos(\alpha)}{MV}[\tan(\gamma)\sin(\mu) + \tan(\beta)] - \frac{T_x\cos(\alpha) + T_z\sin(\alpha)}{MV}\tan(\gamma)\cos(\mu)\sin(\beta) \tag{6}$$

$$\dot{p} = \frac{I_{zz}l + I_{xz}(n + n_T)}{I_{xx}I_{zz} - I_{xz}^2} + \frac{I_{xz}(I_{xx} - I_{yy} + I_{zz})pq + [I_{zz}(I_{yy} - I_{zz}) - I_{xz}^2]qr}{I_{xx}I_{zz} - I_{xz}^2} \tag{7}$$

$$\dot{q} = \frac{1}{I_{yy}}[m + m_T + (I_{zz} - I_{xx})pr + I_{xz}(r^2 - p^2)] \tag{8}$$

$$\dot{r} = \frac{I_{xz}l + I_{xx}(n + n_T)}{I_{xx}I_{zz} - I_{xz}^2} + \frac{[I_{xx}(I_{xx} - I_{yy}) + I_{xz}^2]pq - I_{xz}(I_{xx} - I_{yy} + I_{zz})qr}{I_{xx}I_{zz} - I_{xz}^2} \tag{9}$$

Equations (1-3) govern the magnitude and direction of the velocity vector. They may be derived by considering the aircraft as a point mass and resolving all of the forces acting on the aircraft into three directions. The component in the direction of the velocity vector gives $M\dot{V}$, the component in the upward-pointing normal to V within the vertical plane gives $MV\dot{\gamma}$, and, finally, the horizontal normal to V gives $MV\cos(\gamma)\dot{\chi}$. The variables V, χ, and γ are referred to here as the very slow states, and their rates are controlled by the pilot using the commands α_c, $\dot{\mu}_c$, and T_c to make changes in the magnitude and direction of the lift, drag, and thrust vectors. In this study, a maneuver generator, described in Ref. 2, was implemented to produce α_c, $\dot{\mu}_c$, and T_c. These commands drive the closed-loop aircraft model described in this paper. The commands are designed to produce the following rates in V, χ, and γ:

$$\dot{V}_d = 0.2(V_c - V) \tag{10}$$

$$\dot{\chi}_d = 0.5(\chi_c - \chi) \tag{11}$$

$$\dot{\gamma}_d = 0.5(\gamma_c - \gamma) \tag{12}$$

Equations (4–6) govern the slow states β, α, and μ. Equations (4) and (5) are derived by resolving forces into the body-axis directions to give $\dot{u}$, $\dot{v}$, and $\dot{w}$, which are related to $\dot{\alpha}$ and $\dot{\beta}$ through the relationships $\alpha = \tan^{-1}(w/u)$ and $\beta = \sin^{-1}(v/V)$. Equation (6) is obtained by equating the total angular velocity vector of the aircraft, which has body-axis components p, q, and r, to the rates $\dot{\chi}$, $\dot{\gamma}$, $\dot{\mu}$, $\dot{\beta}$, and $\dot{\alpha}$. Resolving in the direction of V yields $\dot{\mu}$.

The states p, q, and r are governed by Eqs. (7–9), which assume symmetry of the aircraft about the xz plane. These equations are derived from the familiar Euler equations, which equate total moment components to the rate of change of the angular momentum about the respective body axes. These states are assumed to be the fast states because the control surface deflections δ_a, δ_c, δ_r, δ_y, and δ_z have a significant, direct effect on the time derivatives $\dot{p}$, $\dot{q}$, and $\dot{r}$. This is because the control surfaces are configured to produce large moments using relatively small forces. For example, the effect of canard deflections on $\dot{\alpha}$ is very small compared with its effect on $\dot{q}$.

The forces L, D, and Y are assumed to be functions of the states V, β, α and the inputs δ_a, δ_c, and δ_r alone, although more sophisticated models might also include small p, q, and r dependencies. The expressions for T_x, T_y, and T_z, which appear in Eqs. (1–9), were simplified by the assumption that δ_y and δ_z are limited to a maximum deflection of 15 deg, to give the approximate expressions:

$$T_x = T \tag{13}$$

$$T_y = T\delta_y \tag{14}$$

$$T_z = T\delta_z \tag{15}$$

where δ_y and δ_z are specified in radians. The response to throttle commands is modeled as a first-order lag with a time constant of 3 s, whereas the TVC vane deflections δ_y and δ_z are assumed to have a 30 rad/s bandwidth, which is the same as the aerodynamic control surfaces.

Dynamic Inversion Control Law: Inner Control Loops for the States p, q, and r

Having separated states into fast and slow dynamics, feedback is used to provide the system with desirable fast dynamics. The desired closed-loop fast dynamics used in this study are specified by Eqs. (16–18), where the subscript d represents the desired value. The terms p_c, q_c, and r_c are the commanded roll, pitch, and yaw rate given by the slow-state control law shown in Fig. 1:

$$\dot{p}_d = \omega_p(p_c - p) \tag{16}$$

$$\dot{q}_d = \omega_q(q_c - q) \tag{17}$$

$$\dot{r}_d = \omega_r(r_c - r) \tag{18}$$

The bandwidths ω_p, ω_q, and ω_r were set at 10 rad/s, which is about as high as they can be without exciting structural modes or being subject to the bandwidth limitations of the control actuators. Reference 12 shows that it is beneficial to set the bandwidths ω_p and ω_r equal to one another to maintain turn coordination during aggressive rolling maneuvers. It also states that supplementing the dynamics (16–18) with integral action can improve the steady-state performance in the presence of modeling uncertainties. Although integral action was used in the simulations of this paper, it will not be discussed here because it tends to cloud the primary ideas behind the design.

Equations (7–9) can be rewritten in the standard form for the application of dynamic inversion:

$$\begin{bmatrix} \dot{p} \\ \dot{q} \\ \dot{r} \end{bmatrix} = \begin{bmatrix} f_p(\bar{x}) \\ f_q(\bar{x}) \\ f_r(\bar{x}) \end{bmatrix} + \boldsymbol{g}(\bar{x}) \begin{bmatrix} \delta_a \\ \delta_c \\ \delta_r \\ \delta_y \\ \delta_z \end{bmatrix} \tag{19}$$

where $\bar{x}$ is the eight-vector of system states:

$$\bar{x} = [V, \beta, \alpha, p, q, r, \mu, \gamma]^T \tag{20}$$

The $\boldsymbol{f}(\bar{x})$ is a three-vector function with components $f_p(\bar{x})$, $f_q(\bar{x})$, and $f_r(\bar{x})$, whereas $\boldsymbol{g}(\bar{x})$ is a 3×5 matrix function of $\bar{x}$, which relates the five control deflections to the rates $\dot{p}$, $\dot{q}$, and $\dot{r}$. Note that the velocity heading χ is not included in the definition of $\bar{x}$ because $\boldsymbol{f}$ and $\boldsymbol{g}$ are not dependent on heading.

Manipulating Eqs. (7–9) leads to the following expressions for the elements of $\boldsymbol{f}(\bar{x})$ and $\boldsymbol{g}(\bar{x})$:

$$f_p(\bar{x}) = \frac{I_{zz}\hat{l} + I_{xz}\hat{n}}{I_{xx}I_{zz} - I_{xz}^2} + \frac{I_{xz}(I_{xx} - I_{yy} + I_{zz})pq + [I_{zz}(I_{yy} - I_{zz}) - I_{xz}^2]qr}{I_{xx}I_{zz} - I_{xz}^2} \tag{21}$$

$$f_q(\bar{x}) = \frac{\hat{m}}{I_{yy}} + \frac{(I_{zz} - I_{xx})pr + I_{xz}(r^2 - p^2)}{I_{yy}} \tag{22}$$

$$f_r(\bar{x}) = \frac{I_{xz}\hat{l} + I_{xx}\hat{n}}{I_{xx}I_{zz} - I_{xz}^2} + \frac{[I_{xx}(I_{xx} - I_{yy}) + I_{xz}^2]pq - I_{xz}(I_{xx} - I_{yy} + I_{zz})qr}{I_{xx}I_{zz} - I_{xz}^2} \tag{23}$$

where $\hat{l}$, $\hat{m}$, and $\hat{n}$ are defined by

$$\hat{l} = \bar{q}Sb\left[C_{l_\beta}(\alpha)\beta + C_{l_p}(\alpha)\frac{pb}{2V} + C_{l_r}(\alpha)\frac{rb}{2V}\right] \tag{24}$$

$$\hat{m} = \bar{q}S\bar{c}\left[C_m(\alpha)\beta + C_{m_q}(\alpha)\frac{q\bar{c}}{2V}\right] \tag{25}$$

$$\hat{n} = \bar{q}Sb\left[C_{n_\beta}(\alpha)\beta + C_{n_p}(\alpha)\frac{pb}{2V} + C_{n_r}(\alpha)\frac{rb}{2V}\right] \tag{26}$$

The aerodynamic derivatives in Eqs. (24–26) are assumed to be smooth functions of α alone, although this is not a prerequisite for application of the inversion technique. Reference 13 discusses an application of the inversion technique to a table look-up data base, where interpolation over several independent variables is used.

Typical decoupling of symmetric and antisymmetric inputs makes several of the elements of the matrix function $\boldsymbol{g}(\bar{x})$ zero:

$$\boldsymbol{g}(\bar{x}) = \begin{bmatrix} g_{p_{\delta_a}}(\bar{x}) & 0 & g_{p_{\delta_r}}(\bar{x}) & g_{p_{\delta_y}}(\bar{x}) & 0 \\ 0 & g_{q_{\delta_c}}(\bar{x}) & 0 & 0 & g_{q_{\delta_z}}(\bar{x}) \\ g_{r_{\delta_a}}(\bar{x}) & 0 & g_{r_{\delta_r}}(\bar{x}) & g_{r_{\delta_y}}(\bar{x}) & 0 \end{bmatrix} \tag{27}$$

The elements of the matrix $\boldsymbol{g}(\bar{x})$ are of the form

$$g_{p_{\delta_a}}(\bar{x}) = \frac{I_{zz}\bar{q}Sb\,C_{l_{\delta_a}}(\bar{\alpha}) + I_{xz}\bar{q}Sb\,C_{n_{\delta_a}}(\alpha)}{I_{xx}I_{zz} - I_{xz}^2} \tag{28}$$

Equation (19) is inverted to yield Eq. (29), which gives the control deflections necessary to produce the desired angular accelerations of Eqs. (16-18):

$$\begin{bmatrix}\delta_a\\ \delta_c\\ \delta_r\\ \delta_y\\ \delta_z\end{bmatrix} = \boldsymbol{g}_R^{-1}(\bar{x})\left(\begin{bmatrix}\dot{p}_d\\ \dot{q}_d\\ \dot{r}_d\end{bmatrix} - \begin{bmatrix}f_p(\bar{x})\\ f_q(\bar{x})\\ f_r(\bar{x})\end{bmatrix}\right) \tag{29}$$

Here $\boldsymbol{g}(\bar{x})\boldsymbol{g}_R^{-1}(\bar{x}) = I$, where I is a 3×3 identity matrix.

Generically, $\boldsymbol{g}(\bar{x})$ is of rank 3 and, therefore, is right invertible, and the inverse is denoted by $\boldsymbol{g}_R^{-1}(\bar{x})$. The right inverse is not unique because there are many ways in which the five inputs may be used to produce the three desired moments. Substituting the control commands given by Eq. (29) into Eq. (19) produces the desired angular acceleration. We made use of properties of the pseudo-inverse, discussed in Ref. 14, to select a specific right inverse, $\boldsymbol{g}_{\hat{R}}^{-1}(\bar{x})$, which yields the unique input vector u, giving the desired $\dot{p}$, $\dot{q}$, and $\dot{r}$ while also having the minimal Euclidean norm of the weighted input vector $\hat{u}$ defined by Eq. (30):

$$\hat{u} = \begin{bmatrix}\delta_a/\delta_{a\max}\\ \delta_c/\delta_{c\max}\\ \delta_r/\delta_{r\max}\\ \delta_y/\delta_{y\max}\\ \delta_z/\delta_{z\max}\end{bmatrix} \tag{30}$$

With this choice for $\boldsymbol{g}_{\hat{R}}^{-1}(\bar{x})$, the controls are always used with greatest effectiveness in terms of minimizing $\hat{u}$. If a control surface has a large deflection limit, then the penalty for its use is smaller than that of a control having a small deflection limit. One consequence of apportioning the controls in this way is that TVC is used to augment the aerodynamic surfaces even at low angle of attack. This is quite different from the simple α-dependent schedule employed to gang lateral TVC with the rudder in the gain-scheduled control law of Ref. 2. This may explain why control deflections are generally lower with the inversion control law than they are with the gain-schedule control law.

Outer Loops for Control of α, β, and μ

The design of the control laws for the slow states assumes that the fast states track their slowly changing commands exactly. Thus, the design of the slow-state control law is an approximation. It is assumed that the transient dynamics of the fast states occur so quickly that they have negligible effect on the slow states.

By examining Eqs. (4-6), it is seen that the time derivatives of the slow states depend heavily on the fast states p, q, and r. Thus, the commanded values of p, q, and r are used as the inputs in the slow-state control law.

The controller for the slow states was designed by manipulating Eqs. (4-6), which can be rewritten as

$$\begin{bmatrix}\dot{\beta}\\ \dot{\alpha}\\ \dot{\mu}\end{bmatrix} = \begin{bmatrix}f_\beta(\bar{x}_{s_1})\\ f_\alpha(\bar{x}_{s_1})\\ f_\mu(\bar{x}_{s_1})\end{bmatrix} + \boldsymbol{g}_{s_1}(\bar{x}_{s_1})\begin{bmatrix}p\\ q\\ r\end{bmatrix} + \boldsymbol{g}_{s_2}(\bar{x}_{s_1})\bar{u} \tag{31}$$

where $\bar{x}_{s_1}$ consists of the slowly changing states defined by

$$\bar{x}_{s_1} = [V, \beta, \alpha, \mu, \gamma]^T \tag{32}$$

The terms $f_\beta(\bar{x}_{s_1})$, $f_\alpha(\bar{x}_{s_1})$, $f_\mu(\bar{x}_{s_1})$, and $\boldsymbol{g}_{s_1}(\bar{x}_{s_1})$ are given by

$$f_\beta(\bar{x}_{s_1}) = \frac{1}{MV}\bar{q}SC_{Y_\beta}(\alpha)\,\beta\cos(\beta) + \frac{1}{MV} \times [Mg\cos(\gamma)\sin(\mu) - T\sin(\beta)\cos(\alpha)] \tag{33}$$

$$f_\alpha(\bar{x}_{s_1}) = \frac{-1}{MV\cos(\beta)}\bar{q}SC_L(\alpha) + \frac{1}{MV\cos(\beta)} \times [Mg\cos(\gamma)\cos(\mu) - T\sin(\alpha)] \tag{34}$$

$$f_\mu(\bar{x}_{s_1}) = -\frac{g}{V}\tan(\beta)\cos(\gamma)\cos(\mu) + \frac{1}{MV}\bar{q}SC_L(\alpha) \times [\sin(\mu)\tan(\gamma) + \tan(\beta)] + \frac{1}{MV}\bar{q}SC_{Y_\beta}(\alpha)\,\beta\tan(\gamma)\cos(\beta)\cos(\mu) + \frac{T}{MV}\sin(\alpha)[\tan(\gamma)\sin(\mu) + \tan(\beta)] - \frac{T}{MV}\tan(\gamma)\cos(\mu)\cos(\alpha)\sin(\beta) \tag{35}$$

$$\boldsymbol{g}_{s_1}(\bar{x}_{s_1}) = \begin{bmatrix}\sin(\alpha) & 0 & -\cos(\alpha)\\ -\tan(\beta)\cos(\alpha) & 1 & -\tan(\beta)\sin(\alpha)\\ \sec(\beta)\cos(\alpha) & 0 & \sec(\beta)\sin(\alpha)\end{bmatrix} \tag{36}$$

The form of $\boldsymbol{g}_{s_2}(\bar{x}_{s_1})$ is similar to that of $\boldsymbol{g}(\bar{x})$ given in Eq. (27) and will not be discussed further.

The desired $\dot{\beta}$, $\dot{\alpha}$, and $\dot{\mu}$ are specified by the following closed-loop dynamics:

$$\dot{\beta}_d = \omega_\beta(\beta_c - \beta) \tag{37}$$

$$\dot{\alpha}_d = \omega_\alpha(\alpha_c - \alpha) \tag{38}$$

$$\dot{\mu}_d = \frac{4}{s+4}\dot{\mu}_c \tag{39}$$

The bandwidths ω_α and ω_β were set at 2 rad/s, which is sufficiently below the bandwidth of the inner p, q, and r loops to avoid coupling between the inner- and outer-loop dynamics.

The commands β_c and α_c represent the pilot inputs to the rudder pedals and longitudinal stick, respectively. The command $\dot{\mu}_c$ is different in that the bank-angle rate, rather than the bank angle itself, is commanded by the pilot. The command is filtered to give a desired roll-subsidence response of $4/(s+4)$. A direct connection to the 10 rad/s inner loops would give roll response that is overly sensitive to pilot inputs. The roll-rate command $\dot{\mu}_c$ is limited to a maximum of 143 deg s. A separate outer loop to allow μ to track the command μ_c was implemented to drive the $\dot{\mu}$ input, with a constant gain $\omega_\mu = 1.5$ rad/s times the error between μ and μ_c. The μ loop is not part of the onboard flight control system but instead forms a part of the maneuver generator. That is why it is shown dashed in Fig. 1.

The form of $\boldsymbol{g}_{s_1}(\bar{x}_{s_1})$ is defined by kinematics and is identical for any aircraft. This matrix is full rank except when $\cos(\beta) = 0$. The relationship between the steady-state values of the five control surface inputs and the fast states is a nonlinear function of the system states as a result of gyroscopic coupling in Eqs. (7-9). This makes it hard to compute the desired p_c, q_c, and r_c to use as the inputs to the slow-state equations. For this

reason, the small, $g_{s_2}(\bar{x}_{s_1})$ term in Eq. (31) was neglected and the relations given by

$$\begin{bmatrix} \dot{\beta} \\ \dot{\alpha} \\ \dot{\mu} \end{bmatrix} \approx f_s(\bar{x}_{s_1}) + g_{s_1}(\bar{x}_{s_1}) \begin{bmatrix} p \\ q \\ r \end{bmatrix} \tag{40}$$

were used. This is common practice in flight control design.[15,16] The fast-state commands p_c, q_c, and r_c are given by applying inversion to Eq. (40):

$$\begin{bmatrix} p_c \\ q_c \\ r_c \end{bmatrix} = g_{s_1}^{-1}(\bar{x}_{s_1}) \left[\begin{bmatrix} \dot{\beta}_d \\ \dot{\alpha}_d \\ \dot{\mu}_d \end{bmatrix} - f_s(\bar{x}_{s_1}) \right] \tag{41}$$

The simplifications used in Eqs. (40) and (41) neglect the steady-state effects of the inputs δ_a, δ_c, δ_r, δ_y, δ_z on the slow dynamics. This is like assuming that terms such as $C_{L_{\delta_c}}$ and $C_{Y_{\delta_r}}$ are zero in Eqs. (4-6). That is, the control surfaces and TVC produce moments to control $\dot{p}$, $\dot{q}$, and $\dot{r}$, but it is asasumed that they do not produce any forces that have a direct effect on $\dot{\beta}$, $\dot{\alpha}$, $\dot{\mu}$.

The effect on the slow dynamics caused by the approximations can be estimated by examining the longitudinal dynamics only. The exact expression for $\dot{\alpha}$ derived from Eq. (5) is

$$\dot{\alpha} = \frac{-1}{MV}\bar{q}SC_L(\alpha) + \frac{1}{MV}[Mg\cos(\gamma) - T\sin(\alpha)] + q - \frac{1}{MV}\bar{q}SC_{L_{\delta_c}}(\alpha)\delta_c \tag{42}$$

First we substitute the value of δ_c, which is specified exactly by the fast control law:

$$\delta_c = \frac{1}{\bar{q}S\bar{c}C_{m_{\delta_c}}(\alpha)}\left[I_{yy}\dot{q}_d - \bar{q}S\bar{c}C_m(\alpha) - \bar{q}S\bar{c}C_{m_q}(\alpha)\frac{\bar{c}}{2V}q\right] \tag{43}$$

This leads to the exact dynamics:

$$\dot{\alpha} = -\frac{1}{MV} - \bar{q}SC_L(\alpha) + \frac{1}{MV}[Mg\cos(\gamma) - T\sin(\alpha)] + q - \frac{1}{MV}\frac{C_{L_{\delta_c}}(\alpha)}{\bar{c}C_{m_{\delta_c}}(\alpha)}\left[I_{yy}\dot{q}_d - \bar{q}S\bar{c}C_m(\alpha) - \bar{q}S\bar{c}C_{m_q}(\alpha)\frac{\bar{c}}{2V}q\right] \tag{44}$$

which can be written as

$$\dot{\alpha} = \frac{1}{MV}[Mg\cos(\gamma) - T\sin(\alpha)] - \frac{1}{MV}\bar{q}SC_L(\alpha) + \frac{1}{MV} \times \frac{C_{L_{\delta_c}}(\alpha)}{\bar{c}C_{m_{\delta_c}}(\alpha)}\bar{q}SC_m(\alpha) + \left[1 + \frac{1}{MV}\frac{C_{L_{\delta_c}}(\alpha)}{C_{m_{\delta_c}}(\alpha)}\bar{q}SC_{m_q}\frac{\bar{c}}{2V}\right]q - \frac{1}{MV}\frac{C_{L_{\delta_c}}(\alpha)}{\bar{c}C_{m_{\delta_c}}(\alpha)}I_{yy}\dot{q}_d \tag{45}$$

The inner-loop inversion sets $\dot{q} = \dot{q}_d$ so that Eq. (45) can be written simply as

$$\dot{\alpha} = \frac{1}{MV}[Mg\cos(\gamma) - T\sin(\alpha)] - (1+\epsilon_1)\frac{1}{MV}\bar{q}SC_L(\alpha) + (1+\epsilon_2)(q - \dot{q}/z) \tag{46}$$

In the approximation of this paper, the terms ϵ_1 and ϵ_2 were assumed to be negligible, the zero z was assumed to be at infinity, and $q = q_c$ exactly. For the X-31 aircraft model used here, it is found that $\epsilon_1 = -0.021$ and $0.01 < \epsilon_2 < 0.05$. The effect of these small perturbations on the dynamics is negligible and can be canceled in steady state by incorporating integrators into the control law. The zero z is located at $V/0.75$ m, so when $V = 30$ m/s^{-1}, $z = 40$ rad/s. Because the dynamics between q_c and q are $10/(s+10)$, the effect of the nonminimum-phase zero z, having a magnitude in excess of 40 rad/s, is negligible.

The final question is whether the approximation $q = q_c$ is reasonable. If ϵ_1 and ϵ_2 are assumed zero and z is assumed infinite, then the exact dynamics are approximated as

$$\dot{\alpha} = \frac{1}{MV}[Mg\cos(\gamma) - T\sin(\alpha)] - \frac{1}{MV}\bar{q}SC_L(\alpha) + q \equiv f_\alpha(\bar{x}_{s_1}) + q \tag{47}$$

Now, examining the second derivative of α gives

$$\ddot{\alpha} = \nabla_x f_\alpha(\bar{x}_{s_1})\dot{\bar{x}}_{s_1} + \dot{q} \tag{48}$$

Setting q_c in accordance with Eq. (41) gives

$$q_c = \dot{\alpha}_d - \frac{1}{MV}[Mg\cos(\gamma) - T\sin(\alpha)] + \frac{1}{MV}\bar{q}SC_L(\alpha) = \dot{\alpha}_d - f_\alpha(\bar{x}_{s_1}) \tag{49}$$

If it is assumed that $\partial f_\alpha(\bar{x}_{s_1})/\partial\alpha$ is the dominant term in $\nabla_x f_\alpha(\bar{x}_{s_1})$ and that $\dot{\alpha}$ is the dominant term in $\dot{\bar{x}}_{s_1}$, then Eq. (48) can be written as

$$\ddot{\alpha} \approx \frac{\partial f_\alpha(\bar{x}_{s_1})}{\partial\alpha}\dot{\alpha} + \dot{q} \tag{50}$$

Substituting Eq. (17) for $\dot{q}$ and then substituting for q using Eq. (47) and q_c using Eq. (49) yields

$$\ddot{\alpha} \approx \frac{\partial f_\alpha(\bar{x}_{s_1})}{\partial\alpha}\dot{\alpha} + \omega_q\{[\dot{\alpha}_d - f_\alpha(\bar{x}_{s_1})] - [\dot{\alpha} - f_\alpha(\bar{x}_{s_1})]\} = \frac{\partial f_\alpha(\bar{x}_{s_1})}{\partial\alpha}\dot{\alpha} + w_q(\dot{\alpha}_d - \dot{\alpha}) \tag{51}$$

We set $\omega_q = 10$ rad/s and $\dot{\alpha}_d = 2(\alpha_c - \alpha)$ so that Eq. (51) becomes

$$\ddot{\alpha} + \left[10 - \frac{\partial f_\alpha(\bar{x}_{s_1})}{\partial\alpha}\right]\dot{\alpha} + 20\alpha = 20\alpha_c \tag{52}$$

These dynamics are very close to the desired $2/(s+2)$ at frequencies up to about 5 rad/s so long as $\partial f_\alpha(\bar{x}_{s_1})/\partial\alpha$ remains somewhat smaller than 10 rad/s so that the coefficient of $\dot{\alpha}$ in Eq. (52) is approximately 10 rad/s. It is imperative that this

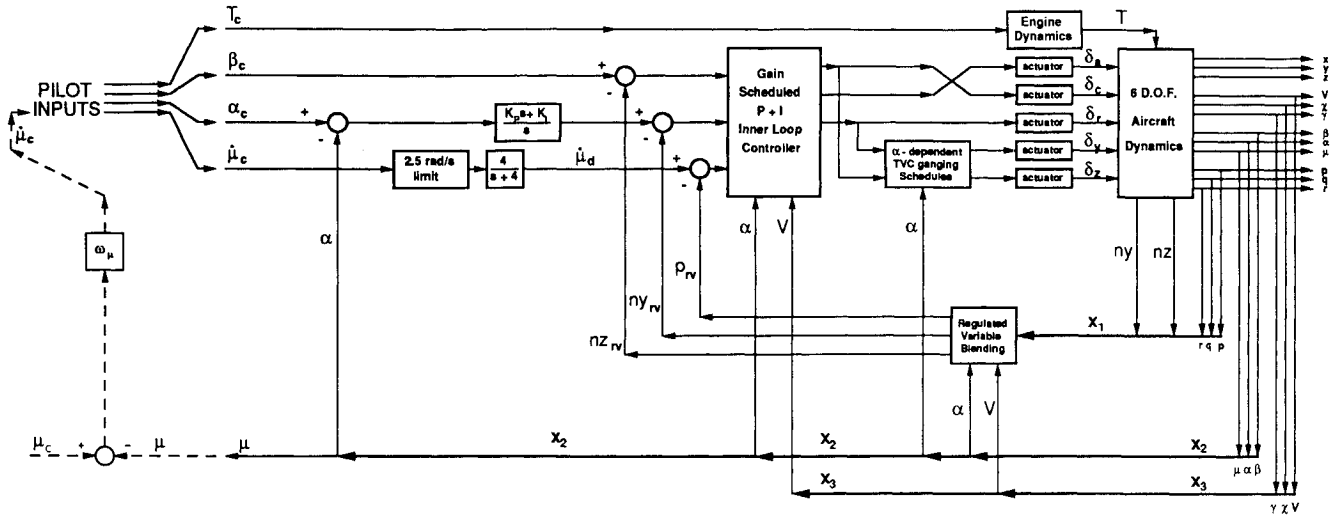

Fig. 2 Configuration of gain-scheduled control laws.

coefficient does not become negative. An approximate bound for $\partial f_\alpha(\bar{x}_{s_1})/\partial\alpha$ is given as

$$\left|\frac{\partial f_\alpha(\bar{x}_{s_1})}{\partial\alpha}\right| \leq \frac{14\ \text{ms}^{-2}}{V} + 0.014\ \text{m}^{-1}V \tag{53}$$

The component in $1/V$ is related to the thrust term in Eq. (34) for $f_\alpha(\bar{x}_{s_1})$, whereas the V component is related to the lift term. The thrust term is much less than 10 rad/s for all V greater than 10 m/s, whereas the lift term is only 4.2 rad/s when V is 300 m/s. If positive of this magnitude, the resulting α dynamics would approximate $20/(s^2 + 6s + 20)$, which has two complex poles with a natural frequency of 4.47 rad/s and a damping factor of 0.67. Note that $\partial f_\alpha(\bar{x}_{s_1})/\partial\alpha$ is negative and hence stabilizing in Eq. (52) for α below the stall. However, it becomes increasingly large and positive beyond the stall. This does not pose a problem, however, because post-stall flight would not be used at speeds in excess of 300 m/s, when $\partial f_\alpha(\bar{x}_{s_1})/\partial\alpha$ becomes significant because of structural and pilot limitations on normal acceleration.

The conclusion of the preceding arguments is that the approximations made for the slow-state control law are justified.

Gain-Scheduled Controller

The baseline control law of Ref. 2 was designed using frequency response techniques applied to linearizations of the nonlinear equations of motion at specified flight conditions. The essential features are shown in Fig. 2. A set of three 10 rad/s bandwidth, inner loops control three regulated variables. The longitudinal regulated variable is a blend of pitch-rate and low-passed normal acceleration and is used to stabilize the longitudinal short period, provide gust rejection, and allow control of angle of attack. The lateral regulated variable is approximately equal to $\dot{\mu}$ for pilot control of bank angle and stabilization of the roll-subsidence and spiral modes. The directional regulated variable is a blend of lateral acceleration—stability-axis, yaw-rate, and bank angle. This stabilizes the dutch roll and provides turn coordination and lateral gust rejection. The design philosophy behind these choices is discussed in more detail in Refs. 2 and 17. The inner loops employ proportional-plus-integral elements that are gain scheduled with angle of attack and dynamic pressure.

The lateral and longitudinal inner loops are driven by outer loops to provide accurate control of α and $\dot{\mu}$. The directional inner loop is simply commanded to zero. The α loop passes the difference α_c and α through a proportional-plus-integral compensator to give a closed-loop bandwidth of 1 rad/s. A μ loop was implemented in the same way as with the dynamic inversion controller described earlier. The μ loop is shown dashed in Fig. 2. The outer-loop gains are not scheduled with flight condition but remain fixed.

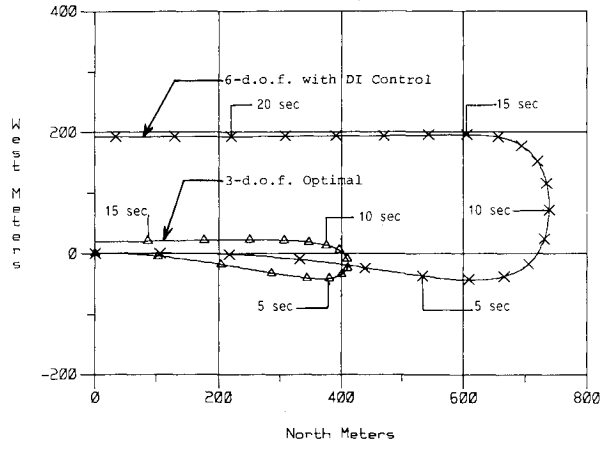

Fig. 3 Optimal 3-DOF vs 6-DOF trajectories with DI control laws, horizontal plane.

Simulated Post-stall Maneuver

Several supermaneuvers taken from data presented in Ref. 18 were simulated using the maneuver generator to provide pilot inputs to the closed-loop aircraft. The optimizations of Ref. 18 are based on point-mass assumptions where the moment equations are accounted for only by trim lift and drag data. A consequence of the point-mass assumption is that the aircraft attitude can be changed instantaneously. On the other hand, the present aircraft model includes rotational dynamics and moments of inertia that preclude instantaneous changes. Hence, the 6-DOF model would not be expected to exactly track the optimal, 3-DOF trajectories of Ref. 18.

The maneuver described in this paper, which is designated EP4.3-2 in Ref. 18, is very aggressive. The objective is a minimal time, 180-deg reversal of the velocity vector with the constraint that the final position and speed be the same as the initial values. In Figs. 3 and 4, the maneuver should be started and completed at the point with coordinates (0,0,0). The optimal trajectory commences with horizontal motion to the north at a speed of 100 m/s and initial altitude of 1000 m. The aircraft makes an immediate steep climb of about 270 m at high α. At the end of the climb, the speed has dropped to 15.8 m/s and α is close to 90 deg. At this point the aircraft makes a rapid rotation about the body x axis and descends along a trajectory similar to the ascent. The maneuver is completed

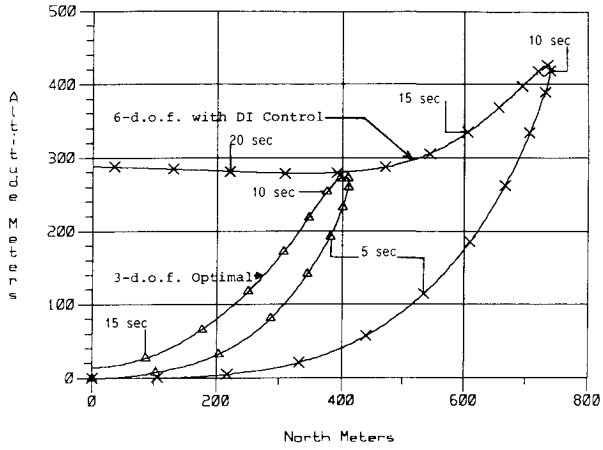

Fig. 4 Optimal 3-DOF vs 6-DOF trajectories with DI control laws, vertical plane.

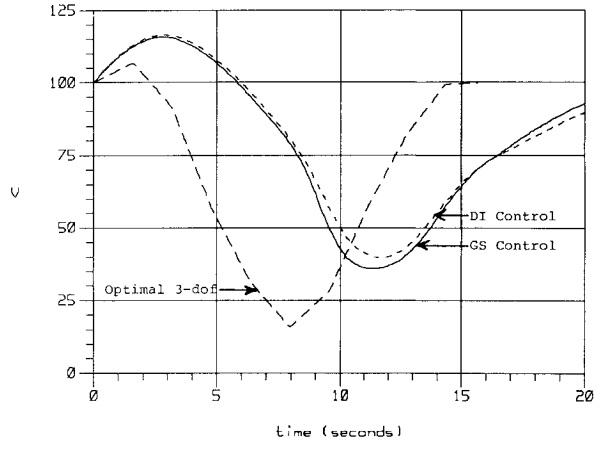

Fig. 5 Speed vs time—optimal 3 DOF, GS 6 DOF, and DI 6 DOF.

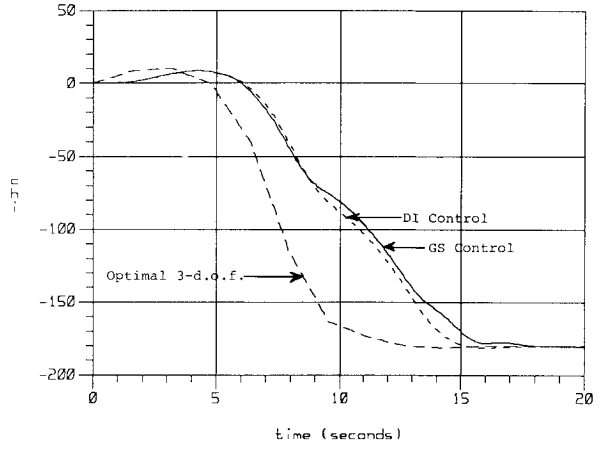

Fig. 6 Velocity heading angle vs time—optimal 3 DOF, GS 6 DOF, and DI 6 DOF.

after 15.9 s, at which point the speed is 100 m/s and the position is (0,0,0) to within a few meters.

It will be seen in Figs. 3 and 4 that our integration of the optimal 3-DOF trajectory does not return exactly to the initial point at $t = 15.9$ s because of integration differences between our simulation and that of Ref. 18. The triangle symbols in Figs. 1 and 2 denote the position at 1-s intervals for our integration of the point-mass trajectory.

The crosses in Figs. 3 and 4 represent the 6-DOF trajectories achieved with the dynamic inversion (DI) control laws. The gain-scheduled trajectories are almost identical, so for clarity they are omitted from the figures. The markers extend for a total period of 22 s from the commencement of the maneuver at the point (0,0,0). The 6-DOF trajectories obtained with both control laws finish in close proximity to one another, and they both "run wide" of the point-mass trajectory. This is partly explained by the fact that after 15.9 s the 3-DOF model has reached its desired position and velocity and subsequent χ and γ commands are zero.

Our point-mass trajectory was based on linear interpolation between the tabulated data points presented in Ref. 18. The data taken from Ref. 18 were the optimal time histories of V, χ, and γ. These data are plotted with long dashes in Figs. 5–7,

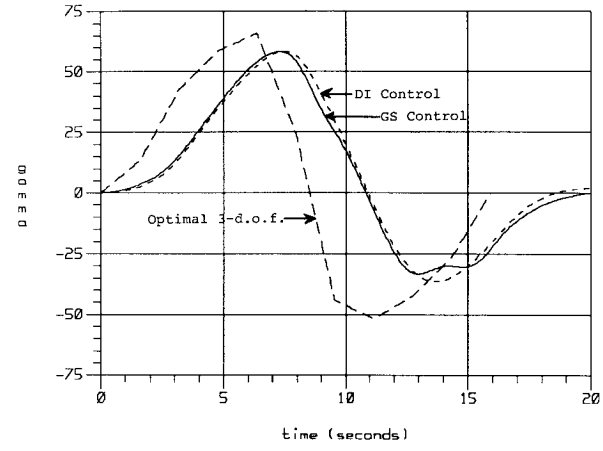

Fig. 7 Flight-path angle vs time—optimal 3 DOF, GS 6 DOF, and DI 6 DOF.

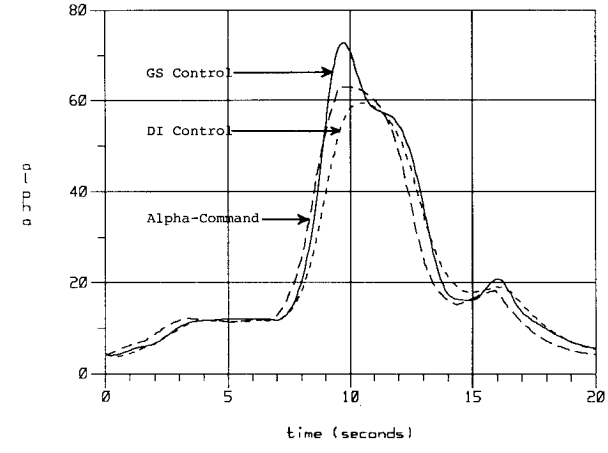

Fig. 8 Angle of attack vs time—GS and DI control laws.

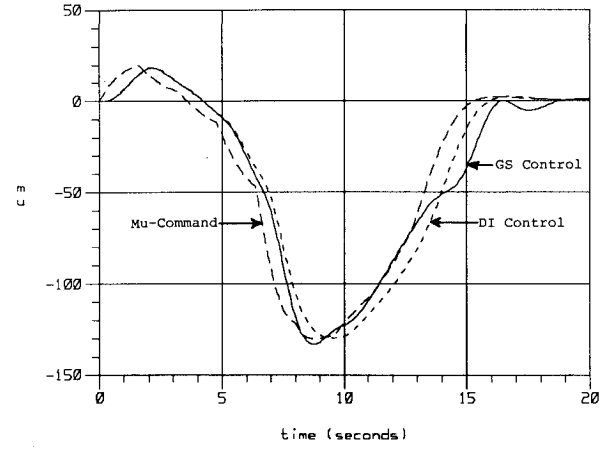

Fig. 9 Bank angle about velocity vector vs time—GS and DI control laws.

where they are compared to the 6-DOF results for GS, solid, and DI with short dashes. It was observed that in 6-DOF simulations, V only dropped to about 40 m/s, whereas the responses in χ and γ lagged the commands by 1.5–2 s. These facts were attributed to the low-bandwidth implementation of the maneuver generator as specified by Eqs. (10–12). The low bandwidth is necessary because in the 6-DOF model it takes a finite, nonzero time to bank, change the angle of attack, and change the engine thrust. The point-mass idealization permits instantaneous changes in any of these quantities.

Figure 8 shows that α reached peak values in excess of 60 deg, which greatly exceeds the 35-deg angle of attack, corresponding to maximum C_L. Thus, the 6-DOF trajectories take place in the post-stall regime. Figures 8 and 9 show that α and μ responses for the GS control law overshot their commands whereas the DI responses did not. The DI and GS controlled responses both lagged the commands in α and μ by about 0.8 s.

The β time histories are plotted in Fig. 10. Here the DI control demonstrated superiority in maintaining peak sideslip at less than 0.25 deg, whereas peak β for the GS control was 11 deg, which is unacceptably high. The peaks in β occurred during and directly following the period at high α but were not present during the period of rapid change in μ. This suggests that the GS control law is not optimized for high α. Figure 11 illustrates that peak ny_{pilot} was more than twice as large for the GS control with peaks about $0.43g$ compared with the DI control with peaks of $0.17g$. The high value of ny_{pilot} produced by the GS control can be explained by the much higher β and the large $\dot{r}$ exhibited in the GS simulation. The time histories of normal acceleration for both DI and GS are similar with peaks of about $3.6g$, which are actually high when the very low speed is considered.

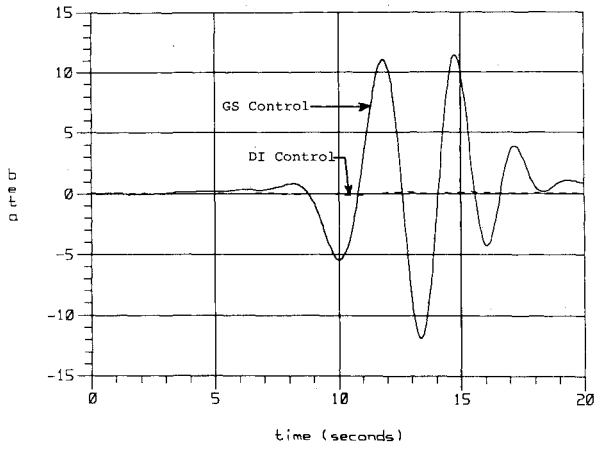

Fig. 10 Sideslip angle vs time—GS and DI control laws.

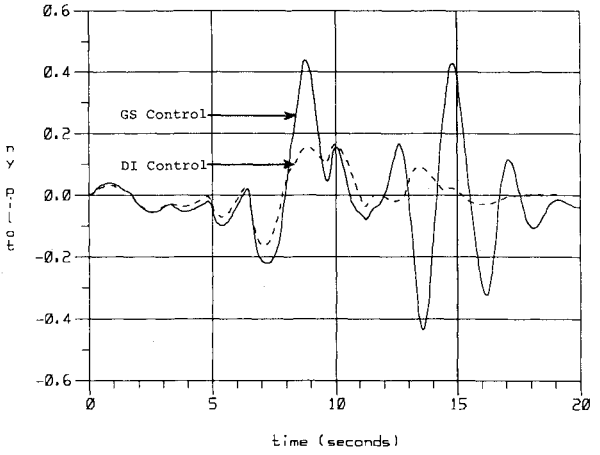

Fig. 11 Lateral acceleration at pilot vs time—GS and DI control laws.

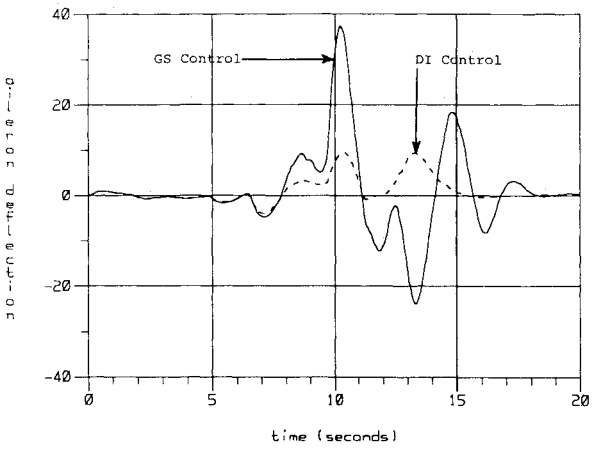

Fig. 12 Aileron deflection vs time—GS and DI control laws.

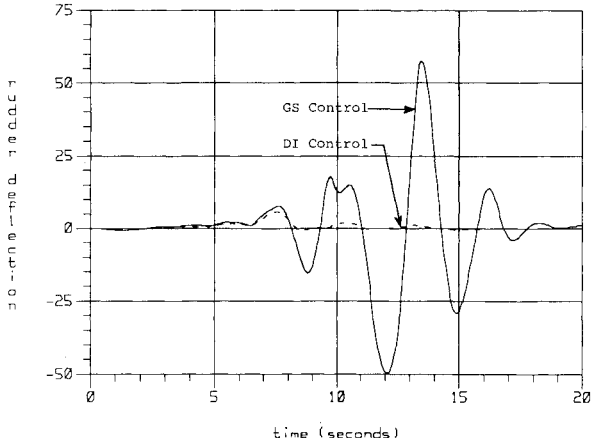

Fig. 13 Rudder deflection vs time—GS and DI control laws.

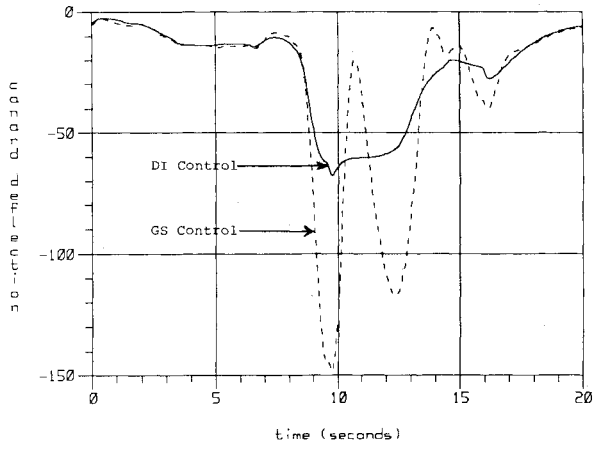

Fig. 14 Canard deflection vs time—GS and DI control laws.

Control surface deflections shown in Figs. 12–14 for both control laws illustrate that the GS control required unacceptably high peak values for all aerodynamic surfaces. These excessive deflections occurred during the time when α and β were close to their maxima. Peak aileron usage for the GS control was 40 deg, four times larger than the DI control. Peak rudder, shown in Fig. 13, was in excess of 50 deg for the GS control, about 10 times larger than the DI control. The lateral TVC deflections for the GS control were acceptable with a peak of 12 deg compared with the DI control peak of 2.6 deg. Peak canard, shown in Fig. 14, for the GS control was −150 deg, which is more than twice the DI control and would

in practice exceed its deflection limit. This indicates that canard control power alone is insufficient for flight in this regime. The DI control law uses normal TVC to augment the canards, but this was not implemented on the GS controller. Normal TVC usage for the DI control was low, with a peak of only 3.7 deg. The GS control had higher peak surface deflections because TVC was only used to augment the rudder, whereas the DI control law exploited all five sources of control power. This gives the DI system an unfair advantage in longitudinal control only. If further work was to be done on the GS design, then normal TVC would be incorporated. This could be accomplished by ganging the normal TVC with the canard in a similar way that lateral TVC was ganged with the rudder. Although the DI control has the additional benefit of normal TVC for pitch, it is worth noting that the GS control still required much larger lateral-directional control deflections despite the use of lateral TVC.

Conclusions

This study has demonstrated the potential of using nonlinear dynamic inversion as a systematic means of deriving control laws for a supermaneuverable aircraft. From our experience with simulation of supermaneuvers, it can be said that the dynamic inversion control laws are superior to our gain-scheduled control laws in providing accurate control of sideslip and lateral acceleration and in reducing control deflections. Clearly, significant improvements could be made to the gain-scheduled laws, such as incorporation of normal TVC, but for a similar level of design effort the inversion control laws provided much better dynamic response.

However, questions remain with regard to robustness properties of the DI control laws. We assumed that the aircraft dynamics could be modeled exactly by our equations of motion. This becomes an increasingly unrealistic assumption at very high angles of attack and when unsteady aerodynamics come into play. It was also assumed that state measurements, such as angle of attack, could be accurately made, which is also questionable at high α. An important contribution in this area would be to select the desired dynamics to endow the closed loop with desirable robustness and performance properties.

Acknowledgment

This research was supported by NASA Langley Research Center under Grant NAG-1-321 with Bart Bacon as technical monitor.

References

[1]Herbst, W. B., "Future Fighter Technologies," *Journal of Aircraft,* Vol. 17, No. 8, 1980, pp. 561–566.

[2]Snell, S. A., Enns, D. F., and Garrard, W. L., "Nonlinear Control of a Supermaneuverable Aircraft," *Proceedings of the AIAA Guidance, Navigation, and Control Conference,* AIAA Paper 89-3486, Washington, DC, 1989.

[3]Morton, G. B., Elgersma, M. R., Harvey, C. A., and Hines, G., "Nonlinear Flying Quality Parameters Based on Dynamic Inversion," Air Force Wright Aeronautical Labs, Technical Rept. AFWAL-TR-87-3079,Wright-Patterson AFB, OH, Oct. 1987.

[4]Elgersma, M. R., "Control of Nonlinear Systems and Application to Aircraft," Ph.D. Thesis, Univ. of Minnesota, Minneapolis, MN, 1988.

[5]Kokotovic, P. V., and Yackel, R. A., "Singular Perturbation of Linear Regulators: Basic Theorems," *IEEE Transactions on Automatic Control,* Vol. AC-17, No. 1, 1972, pp. 29–37.

[6]Chow, J. H., and Kokotovic, P. V., "Two-Time-Scale Feedback Design of a Class of Nonlinear Systems," *IEEE Transactions on Automatic Control,* Vol. AC-23, No. 3, 1978, pp. 438–443.

[7]Menon, P. K. A., Badgett, M. E., Walker, R. A., and Duke, E. L., "Nonlinear Flight Test Trajectory Controls for Aircraft," *Journal of Guidance, Control, and Dynamics,* Vol. 10, No. 1, 1987, pp. 67–72.

[8]Singh, S. N., "Control of Nearly Singular Decoupling Systems and Nonlinear Aircraft Maneuver," *IEEE Transactions on Aerospace and Electronic Systems,* Vol. 24, No. 6, 1988, pp. 775–784.

[9]Kato, O., and Sugiura, L., "An Interpretation of Airplane General Motion and Control as an Inverse Problem," *Journal of Guidance, Control, and Dynamics,* Vol. 9, No. 2, 1986, pp. 198–204.

[10]Asseo, S. J., "Decoupling of a Class of Nonlinear Systems and Its Applications to an Aircraft Control Problem," *Journal of Aircraft,* Vol. 10, No. 12, 1973, pp. 739–747.

[11]Singh, S. N., and Rugh, W. J., "Decoupling in a Class of Nonlinear Systems by State Variable Feedback," *ASME Transactions Series G, Journal of Dynamic Systems, Measurement and Control,* Vol. 94, No. 4, Dec. 1972, pp. 323–329.

[12]Snell, S. A., "Nonlinear Control of Super-Maneuverable Aircraft," Ph.D. Thesis, Dept. of Aerospace Engineering, Univ. of Minnesota, Minneapolis, MN, Oct. 1991.

[13]Bugajski, D. J., Enns, D. F., and Elgersma, M. R., "A Dynamic Inversion Based Control Law with Application to the High Angle of Attack Research Vehicle," *Proceedings of the AIAA Guidance, Navigation, and Control Conference,* AIAA Paper 90-3407, Washington, DC, Aug. 1990.

[14]Strang, G., *Linear Algebra and its Applications,* Academic, New York, 1980.

[15]Hedrick, J. K., and Gopulswany, S., "Nonlinear Flight Control via Sliding Methods," *Journal of Guidance, Control, and Dynamics,* Vol. 13, No. 5, 1990, pp. 850–858.

[16]Lane, S., and Stengel, R. F., "Flight Control Design Using Non-Linear Inverse Dynamics," *Automatica,* Vol. 24, No. 4, 1988, pp. 471–483.

[17]Enns, D. F., Bugajski, D. J., and Klepl, M. J., "Flight Control for the F-8 Oblique Wing Research Aircraft," *Proceedings of the 1987 American Control Conference,* Minneapolis, MN, June 1987, pp. 1112–1119.

[18]Well, K. H., Faber, B., and Berger, E., "Optimale taktische Flugmanoever fuer ein kamfflugzeug der 90er Jahre," Interner Bericht A-52-79/6, DFVLR, Germany, Oct. 1979.